Temperature-driven refacetting phase transition in Pb chains on Si(557)

M. Czubanowski, A. Schuster, H. Pfnür, and C. Tegenkamp
Institut für Festkörperphysik, Leibniz–Universität Hannover, 30167 Hannover, Germany
(Received 11 February 2008; revised manuscript received 1 April 2008; published 13 May 2008)

By using quantitative low energy electron diffraction, we have studied the temperature-driven phase transition of Pb chains grown on Si(557) substrates at a surface concentration of 1.3 ML. This concentration, which is still below one physical monolayer, exhibits a unique switching of electrical conductance from one dimensional to two dimensional above 78 K, which is coupled to this phase transition, and was investigated for this reason. Annealing to 640 K causes a concentration-driven refacetting of the whole surface into large (223) facets at low temperatures, while along the chains a so-called (1,5) linear phase is formed, causing a tenfold periodicity. At T_c=78 K, we analyze a *temperature-driven* order-order transition along the $[\bar{1}\bar{1}2]$ direction in detail, which again turns out to be a refacetting transition. The two-dimensional character of this transition was seen by corresponding structural changes along the $[1\bar{1}0]$ direction as well. Refacetting causes a change in periodicity and destroys the conditions of Fermi nesting necessary for one-dimensional conductance.

DOI: 10.1103/PhysRevB.77.174108 PACS number(s): 73.20.At, 73.21.−b, 68.65.−k, 73.25.+i

I. INTRODUCTION

Confinement effects give rise to fundamental changes in the electronic structure and transport properties in low-dimensional systems. Enhanced correlations between electrons and phonons result in the formation of new quasiparticles, e.g., holons and spinons.[1,2]

As physical model systems in two dimensions, many examples from surface science have been reported in recent years that use, in particular, semiconductor surfaces as templates for the growth of metallic overlayers. In general, this approach allows the control of the morphology, the electronic structure, and the manipulation by, e.g., coadsorption experiments. Characteristic interactions between the adsorbates and the surface reveal the development of metallic surface states. Low dopant concentrations and formation of Schottky barriers at the surface spatially and electronically separate the surface from any bulk and space charge layer contributions. The growth of atomic wires as typical one-dimensional (1D) systems has been found for a variety of materials, such as, e.g., In, Au, Ag, Pt as mono- or submonolayers on Si, and Ge surfaces with different orientations and vicinalities.[3–7] They were generated by self-assembling processes. The 1D character for these systems has been proven by scanning tunneling microscopy (STM) in combination with spectroscopy, revealing a dispersion only along the atomic wires. By using vicinal substrates, even the interchain interaction is tunable and 1D to two-dimensional (2D) transitions can be studied.

Inherent to such low-dimensional systems, however, are instabilities, which lead to metal-insulator transitions for the electronic properties, as, e.g., in Pt/Ge(100).[7,8] These are coupled with structural changes, such as, e.g., period doubling in the simplest case.[9] There are, however, more complicated situations, and the structural nature of transition in low-dimensional systems has been clarified only for very few examples. E.g., for In/Si(111), the $(4\times1)\rightarrow(8\times2)$ transition is close to a displacive phase transition,[10,11] whereas the $(2\times1)\rightarrow c(4\times2)$ transitions of the reconstructed Si(100) and Ge(100) surfaces have an order-disorder character.[12] The $\sqrt{3}\times\sqrt{3}\rightarrow(3\times3)$ transition found for the Sn/Ge(111) system is, however, still under debate.[13]

The Pb system on vicinal Si(557) is not just another example of such transitions, but it turned out to give insight into the properties between one and two dimensions. The adsorption of Pb on this surface leads to a coverage dependent change in step densities that is close to one physical monolayer, coupled with the formation of small Pb covered miniterraces that can be considered as atomic wires.[14] The annealed coverage of 1.3 ML Pb is particularly interesting because electrical conductance in this system reversibly switches from a 2D transport regime into a 1D regime below T_c=78 K, where only along the wire conductance can be measured, while in the perpendicular direction a metal-insulator transition is seen.[15,16] This Pb concentration stabilizes the (223) facet orientation, which corresponds to formation of atomic wires that are four atoms wide with a mesoscopic interchain distance of 1.55 nm.[14,15,17,18] Furthermore, the wires themselves are modulated due to Pb reconstructions on mini-(111) terraces (for details, see Sec. III A). A clear signature for a phase transition has been found not only by transport measurements but also by angle resolved photoemission spectroscopy (ARPES) experiments. Interestingly, ARPES has shown that these wires, contrary to, e.g., Au/Si(557), are two dimensionally coupled and the 1D transport regime is caused by perfect nesting of the Fermi surface at temperatures below T_c=78 K rather than by confinement effects.[19] Due to this strong coupling, it is obvious that any structural change will have drastic consequences toward the electronic properties, but the temperature-driven structural transition has not been identified yet. This is the purpose of this paper.

Former measurements seemed to suggest an order-disorder type of transition, as judged from STM measurements at temperatures well below and above T_c. However, as we will demonstrate below, small changes in average lattice constants and extremely large periodicities are involved, for which spot profile analysis (SPA)–low energy electron diffraction (LEED) turns out to be a much more powerful method than local methods, since long-range correlations can

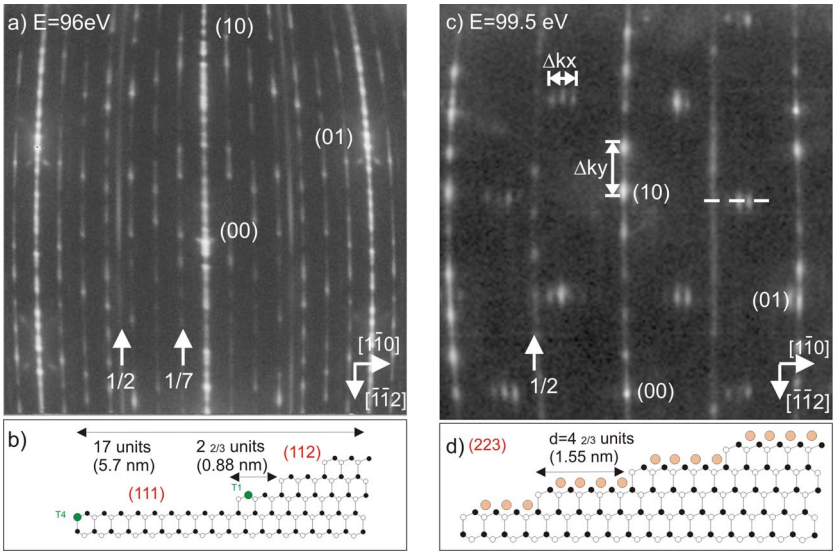

FIG. 1. (Color online) LEED picture of the clean Si(557) surface (a) and after adsorption and thermal annealing of 1.3 ML Pb (c). At the bottom, schematics of the clean (b) and the surface covered by 1.3 ML of Pb are shown (d). The measurements were performed at 40 K.

be still monitored despite strong fluctuations at the atomic scale, expected for these systems above T_c.

In this paper, we present SPA-LEED results that indeed show a clear phase transition at exactly $T_c=78$ K. Induced by thermal activation, the average terrace length is increased; therefore, we call it a refacetting phase transition. The impact of this structural phase transition will be discussed in context with the phase transition seen in conductivity.

II. EXPERIMENTAL SETUP

The sample preparation has been carried out in an UHV chamber operating at a base pressure of 1×10^{-9} Pa. After careful outgassing of the low-doped Si(557) sample, final heating cycles up to 1100 °C have been performed by electron beam heating from the rear of the sample until the Si(557) surface showed a clear LEED pattern of the alternating arrangement of (111) and (112) facets with 7×7 and 2×1 reconstructions, respectively, with the characteristic 17-fold splitting of the spots normal to the step direction. Pb was adsorbed out of a ceramic crucible and the coverage was detected by a quartz microbalance. The exact Pb coverage has been calibrated by using the spot splitting of the domain wall phase formed by the $\sqrt{3}\times\sqrt{3}$ order on the terraces with $\sqrt{7}\times\sqrt{3}$ domain walls, which is also known from Pb/Si(111).[14,20] In a first step, the Pb layers were annealed to 640 K in order to remove the original 7×7 Si structure of the clean terraces and to allow the reordering of the step structure. Further details for the Pb/Si(557) system can be found in Ref. 14.

The sample was mounted on a shielded cryostat so that it could be cooled down to about 4 K by ℓHe. The low temperature regime of up to 300 K was measured by a diode within the cryostat bath, whereas higher temperatures were measured pyrometrically direct on the sample. Both temperature regimes were calibrated in advance by using Ni/NiCr thermocouples on dummy samples. In addition, a power calibration versus steady-state temperatures was carried out.

III. RESULTS

A. Pb-induced chain formation

In order to make the LEED results on the temperature-driven phase transition understandable, which is presented in Sec. III B in detail , we briefly review the essentials obtained around a Pb coverage of 1.30 ML, which is of main importance here. It corresponds to slightly less than one physical monolayer on the terraces.

The clean Si(557) is an unequally stepped surface, which locally consists of (111) and (112) facets, yielding an overall unit cell of 17 a.u. along the $[\bar{1}\bar{1}2]$ direction (5.7 nm) [compare to Fig. 1(b)]. Owing to the (111) miniterrace, LEED reveals uniaxially elongated seventh-order spots, while the half-order spots stem from dimerization at the step edges of the (112) facets. The large unit cell is best seen by the spot splitting of 5.8% surface brillouin zone (SBZ) of the integer spots in the $[\bar{1}\bar{1}2]$ direction. A LEED pattern taken at 96 eV (scattering phase $S=5$ and step height $d=3.14$ Å) is shown in Fig. 1(a). Details about further reconstructions at step edges and terrace sites were recently obtained by STM measurements.[21]

The adsorption of 1.3 ML Pb on Si(557) followed by annealing to 640 K leads to fundamental changes in the surface structure. As evident from the LEED pattern shown in Fig. 1(c), the most striking feature is the spot splitting with a distance between the spots of $\Delta k_y=21.3\%$ SBZ in the $[\bar{1}\bar{1}2]$ direction at temperatures below 78 K. The analysis of the spot profiles has revealed that this splitting corresponds to a (223) facet orientation rather than to a (557) orientation. As schematically depicted in Fig. 1(d), the steps are homogeneously distributed and the terraces are now $4\frac{2}{3}$ a.u., i.e., 1.55 nm wide. The mismatch between both orientations is compensated by terraces with the opposite inclination angle, which do not form larger facets and are, therefore, not visible in LEED. This result of refacetting on a mesoscopic scale is fully supported by recent STM measurements.[17] This phase has been identified as the one responsible for one-dimensional conductance. We will characterize its

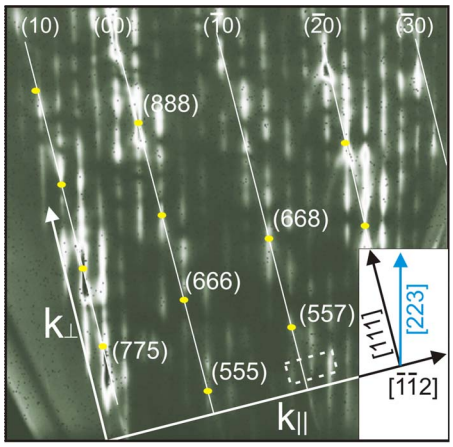

FIG. 2. (Color online) $(k_\perp, k_\parallel)$ plot along the $[\bar{1}\bar{1}2]$ direction showing the regular step train of a (223) facet after adsorption of 1.3 ML Pb on Si(557) and annealing to 640 K. This figure was generated by taking line scans along the central vertical spots of Fig. 1(c) at constant electron energies between 80 and 230 eV. The measurements are taken at $T=40$ K. The dashed square marks the scattering condition, where the step structure has been analyzed as a function of temperature (compare to Fig. 3).

temperature-driven phase transition in Sec. III B.

As is also obvious from Fig. 1(c), superstructure spots at $\sqrt{3}\times\sqrt{3}$ positions appear, which are split by $k_x \approx 10\%$ SBZ in the $[1\bar{1}0]$ direction. We have recently shown that this periodicity is caused by regularly arranged domain walls. On each terrace, this so-called (1,5) linear phase consists of 5 $\sqrt{3}\times\sqrt{3}$, separated by a $\sqrt{7}\times\sqrt{3}$ domain wall. In agreement with previous STM measurements, the chains on adjacent terraces are correlated because the full width at half maximum (FWHM) of these spots periodically varies as a function of the scattering phase.[22]

By varying the Pb concentration on the surface, the interchain distance and the modulation periodicity can be gradually tuned as a function of coverage between 1.2 and 1.6 ML. A detailed phase diagram of the Pb/Si(557) system can be found in Ref. 14. Interestingly, the (557) orientation itself is metastable in the presence of Pb. Among these different Pb phases on Si(557), only the (223) facet structure reveals a nearly equally distributed step structure and only this turns out to be energetically favored, as shown by latest ARPES results.[19] The perfectness of the Pb-induced vicinality is demonstrated in Fig. 2, showing a $(k_\perp, k_\parallel)$ plot, i.e., line scans along the $[\bar{1}\bar{1}2]$ direction were taken at different electron energies and plotted as a grayscale coded image.

Not surprisingly, this particular step structure that strongly deviates from the clean (111) surface is stabilized by the Pb layer. This means that, although STM sees a wirelike structure,[17] these wires must be strongly coupled in two dimensions, which is in agreement with results from a Fermi surface mapping of Pb/Si(557) in the monolayer regime.[19,23] The one-dimensional conductance found for this layer at low temperature below 78 K is thus caused by this particular array of periodic wires resulting in perfect Fermi nesting rather than by localization due to confinement in single wires. The abrupt switching in conductance to a weakly anisotropic two-dimensional system at higher temperature is due to a breakdown of these perfect nesting conditions due to structural changes upon annealing, as we show in Sec. IV. Here, we analyze changes in spot profiles as a function of temperature in detail.

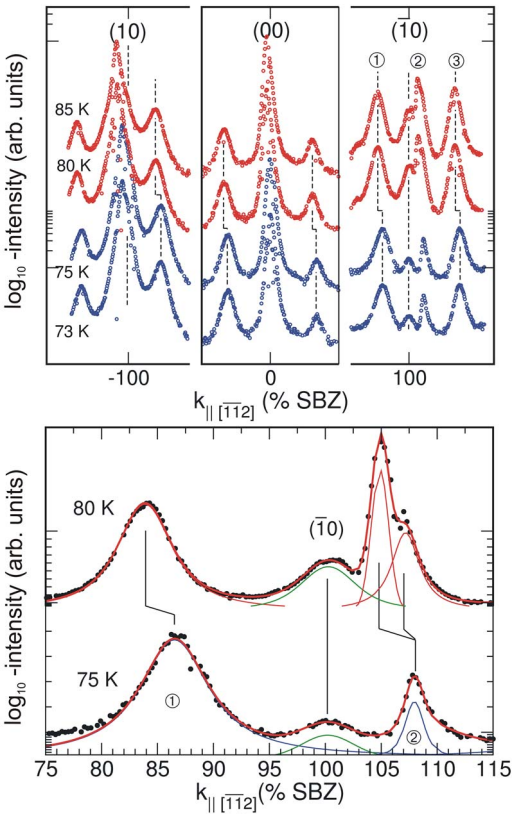

FIG. 3. (Color online) Line scans around the (10), (00), and $(\bar{1}0)$ spots and adjacent diffraction peaks of the step structure along the $[\bar{1}\bar{1}2]$ direction at constant energy ($S=5.1$) but different temperatures around the transition temperature $T_c=78$ K. A magnification of the peak profile of the $(\bar{1}0)$ spot close to the phase transition is shown in the bottom part.

B. Temperature dependent changes in the diffraction pattern

As mentioned, we concentrate on the coverage of 1.30 ML of Pb, i.e., on the (1,5) phase. The upper part of Fig. 3 shows profiles taken at 96 eV around the (10), (00), and $(\bar{1}0)$ spots, respectively, at various temperatures below and above the phase transition observed in conductance. The satellite peaks around these spots are due to the step train of the (223) facet structure. Starting at low surface temperature, changes become obvious in diffraction, when crossing the transition temperature around 78 K. As can be seen there, peaks shift as a whole, which is most obvious at the $(\bar{1}0)$ spot, and partly change shape, while the separation between peaks, in general, is slightly reduced. This indicates that either the facet orientation of the surface changes again upon thermal excitation, or that a phase equilibrium between different facet orientations is established above the phase transition.

In order to understand the nature of this phase transition in more detail, we first test the hypothesis that the average inclination of the surface can also be changed by temperature. For that purpose, we investigated the spot profiles in those parts of k space in more detail where the changes are most prominent.

This is the case for the $(\bar{1}0)$ spot, for which a magnification of the line scans close to T_c is shown in the lower part of Fig. 3. Below T_c, the part of the profiles shown there can be well described by three diffraction peaks (blue curves, denoted by 1 and 2). The electron energy of 96 eV is almost an out-of-phase scattering condition for the first-order spot with respect to a step height of 3.14 Å between (111) terraces (green curve), as can be seen by the almost symmetric relative positions of the step train peaks with respect to the $(\bar{1}0)$ peak. This small $(\bar{1}0)$ peak would not be present for a homogeneously stepped surface but exists due to small inhomogeneities on the surface or pinned steps yielding larger and uncorrelated (111) terraces. A comparison of intensities at many different electron energies shows that these larger (111) terraces cover less than 10% of the surface area. For the present purpose, however, their $(\bar{1}0)$ diffraction peak, which is fixed in k space, serves as a calibration point in reciprocal space.

The varying FWHMs of peaks 1 and 3 compared to peak 2 directly reflect the finite variance of the terrace length distribution.[24] Assuming a Poisson distribution for the terrace length around a mean value, the FWHM of the diffraction peaks depends on the variance, but also on the distance, Δk, to the next Bragg point as FWHM $\propto(\Delta k)^2$. The detailed analysis of the broadening of the FWHM with respect to the scattering phase relative to the next in-phase condition allows us to calculate the variance. Following the analysis described in Ref. 24, the average variance is $\sigma \approx 0.2a$, assuming a FWHM of 5% SBZ of the broad peaks at a scattering phase difference of around π with respect to the (557) Bragg point.

Above T_c, the diffraction peaks of the step train shift relative to the $(\bar{1}0)$ diffraction peak, but are also split or broadened. Examples for these two cases are again seen at the bottom of Fig. 3. Peak 2 shifts closer to the Bragg peak so that splitting into two peaks can be observed. The splitting is around 3% SBZ. On the other hand, a splitting of peak 1 cannot be resolved due to broadening. These shifts, splitting, and broadenings are reversible and no further changes in shape or position were found while changing the substrate temperature between 4 and 100 K. All changes in positions, temperature dependent splittings, and associated changes of half-widths are compatible with a transition from the (223) facets to an average (17 17 25) orientation, as will be demonstrated below.

A schematic of the Ewald construction for the (223) and (17 17 25) facet structures is shown in Fig. 4(a). The parts that correspond to the scattering conditions of the line scans presented in Fig. 3 are enlarged in Fig. 4(b) for below T_c and in Fig. 4(c) for above T_c. As shown in this schematic, the shift and spot splitting of peak 2 in Fig. 3 above the phase transition is caused by the transition to a high index surface with an inclination in between the (557) and the (223) orientation of the clean and the Pb covered surface at low temperatures, respectively. A (17 17 25) facet structure yields a splitting between two (17 17 25) rods of $\frac{1}{6}\frac{1}{\Gamma_{223}}=3.5\%$SBZ, very close to our finding.

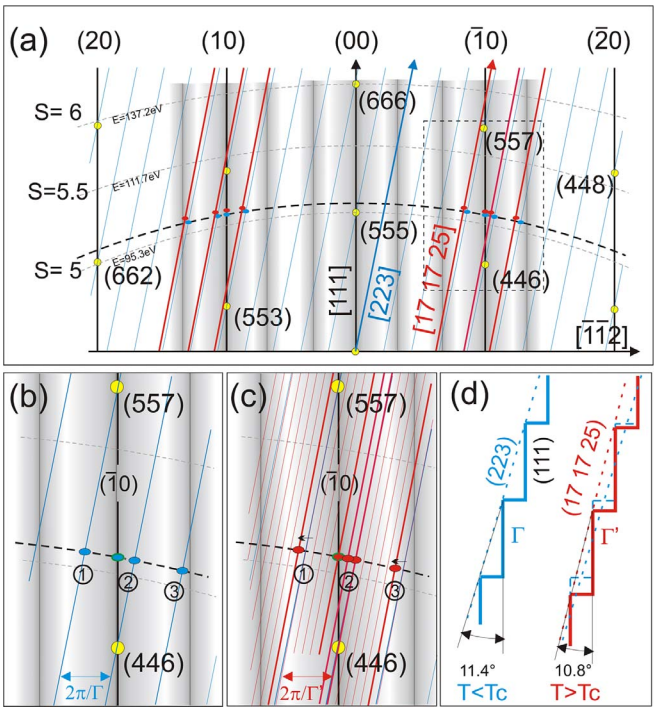

FIG. 4. (Color online) (a) Ewald construction of the diffraction rods as seen by experiments shown in Fig. 2. The blue lines represent the (223) facet structure below T_c, while the facet rods of the high index commensurate (17 17 25) orientation are marked in red. (b) and (c) show magnifications of the area in (a) marked by dashed lines below and above T_c for the (223) and (17 17 25) facet structures, respectively. The numbers correspond to the numbers in Fig. 3. The intensity modulation of the step train spots by the form factor of a single terrace is indicated by the shaded intensity oscillations implying that only the thick red lines in (c) can be observed at the scattering conditions of Fig. 3. (d) Schematic drawing of the two step configurations illustrating the increase in the *average* terrace lengths above T_c.

As can be seen from Figs. 4(b) and 4(c), the rods nicely explain the shifts of the step diffraction peaks and even the splitting of the step peak denoted by 2 and changes of half-widths at others. Because of the chosen scattering condition, this diffraction peak shifts to a condition close to in-phase scattering, i.e., the influence of the variance in the terrace size distribution is small enough so that the peaks can be resolved. In contrast, step diffraction spots of higher order appear only broadened (1 and 3) and a substructure cannot be resolved. Furthermore, the modulation of the intensity distribution by the form factor of the (111) miniterraces suppresses further diffraction peaks of the high index facet structure.

Although the general behavior of the changes in the diffraction pattern can be explained by this change of average facet orientation, a direct measurement of the change of inclination angle can only be obtained by energy dependent measurements. Therefore, we have measured the spot split-

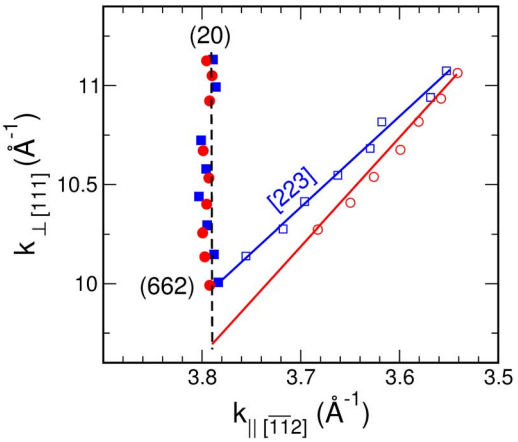

FIG. 5. (Color online) Peak positions of (223) step spot (open symbols) with respect to the (111) rod (closed symbols) measured at 4 (squares) and 80 K (circles) at the (662) Bragg point.

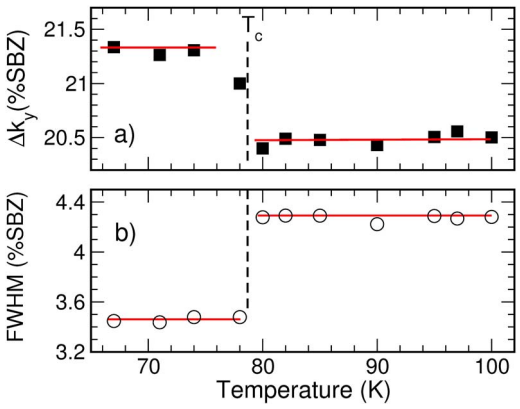

FIG. 6. (Color online) (a) Variation in spot separation as a function of temperature for step-induced diffraction peaks taken at 96 eV (splitting not resolvable here). (b) FWHM of a step diffraction peak around the $\bar{2}0$ spot vs temperature. In both cases, the discontinuity at T_c is clearly visible.

ting as a function of energy for two different temperatures. Exemplarily, the energy dependent splitting of the (20) rod around the (662) Bragg point and the adjacent step train peak are plotted in Fig. 5 for below and above T_c. The scattering conditions are given in Å^{-1} to directly allow the determination of the facet orientation via $\tan(\theta)=\frac{k_\parallel}{k_\perp}$. The electron energy was varied between 96 and 127 eV, which correspond to phases $S=5$ and $S=5.75$, respectively. For the measurement at 4 K, the angle between the rods is $\theta=11.4° \pm 0.3°$, which is in almost perfect agreement with a (223) facet as already judged from the spot splitting Δk_y. At 80 K, this angle changes to $10.5° \pm 0.3°$, which is within error bars compatible with a (17 17 25) orientation. This directly proofs the temperature dependent reorientation of the whole surface and excludes demixing of different facet orientations on the surface.

To further prove our model and to determine the exact phase temperature, we have analyzed the spot separation as a function of substrate temperature for step-induced diffraction spots for which splitting is not resolvable [see Fig. 6(a)]. This is the case for the majority of spots. However, if the (223) facet orientation is replaced by a high index orientation, the nonresolved peak must contain more than one diffraction spot so that their FWHM must increase. This is exactly what we see. An example is shown in Fig. 6(b). These plots directly demonstrate that both the changes in peak separation and in half-width are directly related to the phase transition at 78 K. Both results qualitatively agree for the FWHM and for the peak splitting even quantitatively with our suggested model: The spot splitting $\Delta k_y=2\pi/\Gamma$ of 21.3% SBZ, i.e., of the (223) step train structure, remains constant up to a temperature of 75 K, while above 78 K it changes to 20.5% SBZ, i.e., close to five unit cells per terrace on average. The clean Si(557) surface has a nominal terrace width of $5\frac{2}{3}$ unit cells, which corresponds to 17.6% SBZ spot splitting and therefore can be well discriminated. This small decrease in the spot splitting is fully consistent with the model schematically sketched in Fig. 4(d).

Since diffraction reveals only the average of a quantity, the obviously incommensurate value for the spot splitting above T_c is the effect of measuring the Fourier transform of a terrace size distribution on a discrete lattice. On average, one row of atoms is added to six (223) terraces, and this correlation must be maintained over several of these large units in order to identify separated diffraction peaks. Both static disorder and thermal fluctuations reduce this order. Consequently, not all diffraction rods of the high index commensurate phase can be detected but only those close to Bragg points, as demonstrated by the spot splitting seen in Fig. 3. For other scattering conditions, this structural transition is seen only by a change in the FWHM due to the finite variance in the terrace size distribution. Exactly at T_c, the FWHM changes to a higher value and remains constant up to 100 K. Fluctuations around the phase transition temperature should cause higher FWHM values only at T_c. The abrupt change seen in Fig. 6 points toward a first-order phase transition, as one might intuitively expect also from the transport measurements, although the conductance itself is not directly related to the order parameter.

The observed changes at the structural phase transition at 78 K are not limited to the average terrace width. We also observed small changes in the domain wall separation of the original Pb-induced (1,5) phase along the terraces, which demonstrate that couplings between terraces and the associated phase transitions cannot be treated as one dimensional, in agreement with latest ARPES measurements.[19] Figure 7(a) shows the spot splitting of the domain wall spots *along the* $[1\bar{1}0]$ *direction* as a function of temperature revealing a 4% increase of the average domain wall separation at T_c. In Fig. 7(b), we have plotted the peak position of the simultaneously measured $\sqrt{3}$ spot. The fact that the position does not shift with temperature excludes any instrumental effects upon annealing the sample.

IV. DISCUSSION

Our results that we have just presented show that for the physical monolayer of Pb [1.30 ML Pb with respect to the Si(111) surface concentration], a prominent phase transition

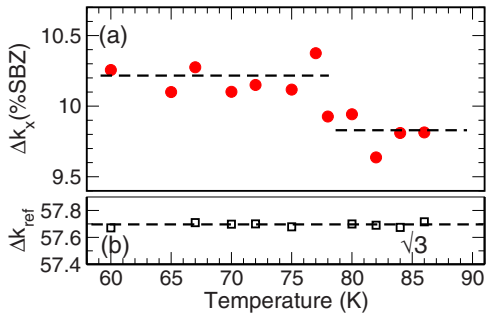

FIG. 7. (Color online) (a) The domain wall splitting Δk_x along the $[1\bar{1}0]$ direction as a function of temperature. (b) Peak position of the $\sqrt{3}$ position vs temperature.

occurs at T_c=78 K, where both the distances of adjacent steps and of domain walls in the direction along the steps abruptly increase by about 4% on average. It is worth pointing out, however, that no local expansions of lattice constant are involved in this phase transition and all atoms remain on their crystalline sites. It is thus a type of order-order phase transition, in which only the average inclination of the facets on the surface changes at T_c. We call this a refacetting surface phase transition. From the small background intensity and the absence of clear fluctuation-induced contributions to the diffraction profiles, we conclude that this phase transition is of first order. This fits to the abrupt change of the ordering parameter, i.e., of the average terrace length.

Due to the large periodic (average) units and their small changes involved in this phase transition, it would be extremely difficult to detect such a transition with a local method, such as tunneling microscopy, and has indeed not been seen.[15,17] It means to add one row of atoms every six terraces *on average* in a fluctuating system. Therefore, averages over several hundred terraces are necessary to safely detect such a small change, which in addition is not static on STM time scales. The present study has nicely demonstrated that such a clarification of the nature of a phase transition on a mesoscopic scale can be reliably done only by diffraction.

Pb in the monolayer regime on the Si(557) surface has the intriguing effect that it stabilizes step formation and, thus, the formation of facets with step densities higher than that of the macroscopic orientation.[14] The coverage dependent variation in step density is compatible with a model that assumes that step decoration, however, is avoided, so that an increase in Pb concentration leads to a reduction in step density until formation of a second layer starts and the steps are also filled with Pb at concentrations above 1.4 ML. As concluded from recent ARPES measurements for the 1.30 ML concentration of Pb,[19] there is a clear electronic component in the stabilization of enhanced step densities, at this concentration of the (223) facet orientation. At E_F, a gap of around 20 meV is opened in the $[\bar{1}\bar{1}2]$ direction for the Pb-induced (223) facets due to perfect Fermi nesting for exactly this orientation. A gap of this size is expected for a transition temperature of 78 K seen here and also in conductance measurements.

Excitation of electrons across this gap is obviously coupled with a destabilization of the (223) facet in favor of the (17 17 25) facet with a lower step density. While this small change in periodicity leads to a breakdown of the Fermi nesting condition and to a transformation of one-dimensional to two-dimensional conductance, it directly demonstrates the strong coupling between electronic and vibrational degrees of freedom.

Therefore, lattice entropic effects are also not negligible. The increase in the average interterrace distance by about 4% can be interpreted as a result of an increased entropic repulsion due to an enhanced meandering of steps.[25] Strong fluctuations are indeed expected for Pb at upper step sites because of the low Debye temperature and are supported by recently performed STM measurements that showed the $3\times3\rightarrow\sqrt{3}\times\sqrt{3}$ transition for the Pb/Si(111) system.[26] On the other hand, this entropic contribution is monotonously increasing with temperature and does not account for the preferred average terrace length at high temperature seen in our experiments.

To some extent, however, an increase in temperature acts in the same direction as an increase in Pb concentration, since both an increase of concentration and the temperature enhanced entropic interactions lead to an increase in step-step repulsion. This is seen from measured changes in the vicinality as a function of coverage at a constant temperature of 70 K. Starting with the (1,5) phase, the Pb coverage was increased up to 1.42 ML in steps of 0.01 ML, which resulted in the same change in the vicinality of the (223) facet as that found above by increasing T above T_c at the constant coverage of 1.3 ML.[22]

In contrast, the decrease in the domain wall splitting along the terraces by approximately 4% above T_c would correspond, according to our coverage calibration,[14] to a change by only 0.01 ML Pb. This puzzling finding is consistent with the coverage dependent changes in the $[\bar{1}\bar{1}2]$ direction, assuming that only the (light) domain walls suffer from the excess Pb, whereas the $\sqrt{3}\times\sqrt{3}$ are left unchanged, supposing a homogeneous distribution along the $[1\bar{1}0]$ direction.

V. SUMMARY

Summarizing, we studied a temperature-driven structural phase transition observed for 1.3 ML Pb adsorbed on Si(557), which was identified as a refacetting phase transition. The annealed Pb layer causes a refacetting of the initial inclination into a (223) facet structure at low temperatures. Increasing the temperature leads to the formation of high index facets, which we identified as (17 17 25) facets. These results demonstrate the close electronic and lattice vibrational coupling in these low-dimensional systems. Both electronic and entropic contributions that lead to an order-order transition were identified. Furthermore, from a mesoscopic point of view, the energetics might be described in terms of surface stress, i.e., the difference in surface stress of the (223) facetted areas and larger (111) terraces may lead, in addition, to a reduction of the free energy. However, to elucidate the precise interplay of these different energetic contributions, theoretical calculations are necessary.

ACKNOWLEDGMENTS

The financial support by the Deutsche Forschungsgemeinschaft is gratefully acknowledged.

[1] J. Voit, Rep. Prog. Phys. **58**, 977 (1995).
[2] S. Roth and C. Caroll, *One Dimensional Metals* (Wiley-VCH, Weinheim, 2004).
[3] J. R. Ahn, H. W. Yeom, H. S. Yoon, and I.-W. Lyo, Phys. Rev. Lett. **91**, 196403 (2003).
[4] J. N. Crain, A. Kirakosian, K. N. Altmann, C. Bromberger, S. C. Erwin, J. L. McChesney, J.-L. Lin, and F. J. Himpsel, Phys. Rev. Lett. **90**, 176805 (2003).
[5] J. N. Crain and F. J. Himpsel, Appl. Phys. A: Mater. Sci. Process. **82**, 431 (2006).
[6] U. Schwingenschlögl and C. Schuster, Europhys. Lett. **81**, 26001 (2008).
[7] O. Gurlu, O. A. O. Adam, H. J. W. Zandvliet, and B. Poelsema, Appl. Phys. Lett. **83**, 4610 (2003).
[8] N. Oncel, A. van Houselt, J. Huijben, A.-S. Hallbäck, O. Gurlu, H. J. W. Zandvliet, and B. Poelsema, Phys. Rev. Lett. **95**, 116801 (2005).
[9] E. Peierls, *Quantum Theory of Solids* (Clarendon, Oxford, 1955), p. 108.
[10] H. W. Yeom, S. Takeda, E. Rotenberg, I. Matsuda, K. Horikoshi, J. Schaefer, C. M. Lee, S. D. Kevan, T. Ohta, T. Nagao, and S. Hasegawa, Phys. Rev. Lett. **82**, 4898 (1999).
[11] J. R. Ahn, J. H. Byun, H. Koh, E. Rotenberg, S. D. Kevan, and H. W. Yeom, Phys. Rev. Lett. **93**, 106401 (2004).
[12] Y. Nakamura, H. Kawai, and M. Nakayama, Phys. Rev. B **55**, 10549 (1997).
[13] J. M. Carpinelli, H. H. Weitering, E. W. Plummer, and R. Stumpf, Nature (London) **381**, 398 (1996).
[14] M. Czubanowski, A. Schuster, S. Akbari, H. Pfnür, and C. Tegenkamp, New J. Phys. **9**, 338 (2007).
[15] C. Tegenkamp, Z. Kallassy, H. Pfnür, H.-L. Günter, V. Zielasek, and M. Henzler, Phys. Rev. Lett. **95**, 176804 (2005).
[16] C. Tegenkamp, Z. Kallassy, H.-L. Guenter, V. Zielasek, and H. Pfnür, Eur. Phys. J. B **43**, 557 (2005).
[17] H. Morikawa, K. S. Kim, D. Y. Jung, and H. W. Yeom, Phys. Rev. B **76**, 165406 (2007).
[18] C. Tegenkamp and H. Pfnür, Surf. Sci. **601**, 2641 (2007).
[19] C. Tegenkamp, T. Ohta, J. L. McChesney, H. Dil, E. Rotenberg, H. Pfnür, and K. Horn, Phys. Rev. Lett. **100**, 076802 (2008).
[20] K. Budde, E. Abram, V. Yeh, and M. C. Tringides, Phys. Rev. B **61**, R10602 (2000).
[21] S. A. Teys, K. N. Romanyuk, R. A. Zhachuk, and B. Z. Olshanetsky, Surf. Sci. **600**, 4878 (2006).
[22] A. Schuster, M. Czubanowski, H. Pfnür, and C. Tegenkamp (unpublished).
[23] K. S. Kim, H. Morikawa, W. H. Choi, and H. W. Yeom, Phys. Rev. Lett. **99**, 196804 (2007).
[24] J. Wollschläger and C. Tegenkamp, Phys. Rev. B **75**, 245439 (2007).
[25] X. S. Wang, J. L. Goldberg, N. C. Bartelt, T. L. Einstein, and E. D. Williams, Phys. Rev. Lett. **65**, 2430 (1990).
[26] I. Brihuega, O. Custance, R. Perez, and J. M. Gomez-Rodriguez, Phys. Rev. Lett. **94**, 046101 (2005).